Influence of carbon nanotubes on the plasma electrolytic oxidation process of aluminum under “soft” sparking conditions

Corentin da Silva Tousch, L. Magniez, S. Fontana, G. Marcos, C. Hérold, G. Henrion, T. Czerwiec, J. Martin

Influence of carbon nanotubes on the plasma electrolytic oxidation process of aluminum under “soft” sparking conditions.

C. Da Silva Tousch[a], L. Magniez[a], S. Fontana[a], G. Marcos[a,b], C. Hérold[a], G. Henrion[a,b], T. Czerwiec[a,b], J. Martin[a,b*]

[a] Université de Lorraine, CNRS, IJL, F-54000 Nancy, France

[b] Université de Lorraine, Laboratoire d'Excellence Design of Alloy Metals for low-mAss Structures ('LabEx DAMAS'), F-57045 Metz, France

*Corresponding author: julien.martin@univ-lorraine.fr

Abstract:

Plasma electrolytic oxidation of aluminum (PEO) was performed with dispersed multi-walled carbon nanotubes (MWCNTs) into the electrolyte. The effect of the carbon nanotubes concentration, as well as that of the electrical processing conditions, on the PEO process was investigated. From the point of view of the electrical response of the process, results show that the "soft" sparking regime appears earlier in presence of MWCNTs. The process time at which the transition to the "soft" regime occurs decreases linearly with the increase in the MWCNTs concentration. Over a concentration threshold, depending on the applied pulse bipolar current waveform, the PEO process is inhibited. The dispersion of MWCNTs in the electrolyte results in thicker but more porous alumina layers. More specifically, the proportion of the α-alumina phase relative to the γ-alumina phase decreases with the increase in the MWCNTS concentration. Results are explained by considering the increased coating growth kinetics and lower heat accumulation from MWCNTs addition. Finally, the present study gives new insights into the right management of the PEO process under "soft" sparking regime with dispersed carbon-based nanoparticles in the electrolyte.

Keywords:

aluminum; carbon nanotube (CNT); plasma electrolytic oxidation (PEO); micro-arc oxidation (MAO); “soft” sparking regime; alumina

1. Introduction

Plasma electrolytic oxidation (PEO), also known as micro-arc oxidation (MAO), is a plasma-assisted electrochemical process that allows the surface of various lightweight metals (e.g. Al, Ti, Mg) to be converted in their respective oxide. Unlike conventional anodizing methods, the PEO process is conducted under high current and high voltage resulting in the repetitive dielectric breakdowns of the growing oxide layer and the ignition of micro-discharges over the processed surface [1]. These micro-discharges allow the growth of the oxide layer to continue through various mechanisms involving disrupting, vaporizing, melting, oxidizing, and quenching of the metallic oxide [2]. Although the micro-discharges are necessary to promote the oxide growth, intense micro-discharges have nevertheless a detrimental effect on the final morphology of the grown oxide. Indeed, by introducing excessive thermal and mechanical stresses in the oxide layer, they usually result in the formation of large open pores, thus reducing the wear and corrosion resistances of the produced oxide coatings [3]. In order to better control the micro-discharge appearance, the PEO process can be carried out under bipolar current. It allows the micro-discharges to appear only during the anodic half-period of the current, thus reducing the detrimental effects that are usually observed with DC power supplies [4-6].

Additionally, under bipolar current conditions, the anodic and cathodic periods of the current can be adjusted asymmetrically by setting independently their respective amplitude and duration. A relevant parameter that takes into account this asymmetry is defined as the anodic to cathodic charge quantity ratio. By setting this ratio below 1, when the anodic charge quantity is lower than the cathodic one, Mecuson *et al.* established that a transition from the conventional arc sparking regime to the “soft” sparking regime can occur in the course of the treatment [4]. From the point of view of the process, this transition to the “soft” sparking regime is marked by three main features, namely (i) a gradual decrease in the anodic voltage

amplitude, (ii) a reduction of the acoustic emission issued from the PEO process itself and (iii) a change in the spatial distribution of the micro-discharges over the surface, often leading to a decrease in their brightness [4, 7, 8]. From the point of view of the produced protective coating, the scientific literature is not unanimous on the quality of the coatings produced within this specific "soft" regime. For Song *et al.*, for example, this "soft" sparking regime results in the formation of thicker oxide layers with smaller porosities than under conventional "arc" sparking regime [9]. Cross-section examinations in a study involving ^{18}O tracer emphasized that upon reaching the transition to "soft" sparking, coating growth mainly continues inwards at the interface between the oxide and the substrate [10]. This is also supported by the gradual disappearance of the "pancake" structure at the topmost surface of the coating indicating that coating growth is not driven by the eruption and solidification of molten oxide anymore. The "soft" sparking regime also favors lower energy consumption due to a gradual decrease in the anodic voltage with the processing time [11]. Conversely, Martin *et al.* reported in some cases a slower growth rate under "soft" sparking and the formation of highly irregular coatings [8]. In some cases, the coating thickness can be uneven over the sample surface with thicker coating at the edges than in the center [2, 12]. Anyway, the coating usually remains more spatially uniform when compared to the "arc" regime [13].

Several process parameters such as the anodic current density, the current pulse frequency and even the distance between electrodes have been identified as influencing the transition from the arc to the "soft" sparking regime. [7]. Although the appearance of the "soft" regime has extensively been studied for aluminum substrates [14-16], it remains that magnesium, titanium and zirconium substrates can also manifest similar behaviors under specific conditions [17-21]. Qin Tang *et al.* [19] pointed out the role of ionic salts in the electrolyte composition on the arc to "soft" regime transition. In a previous work, the ageing of the electrolyte was also shown to influence this transition [22].

Meanwhile, a growing interest for PEO treatments involving solid particle incorporation has recently been observed. Numerous works are devoted to PEO coatings produced in electrolytes containing a dispersion of micro- or nano-particles (see for instance the review papers from Lu *et al.* [23] or O'Hara *et al.* [24]). Although the incorporation mechanisms of the particles into the growing coating are still debated, a wide variety of particles have been used in order to improve the properties of the generated coating. Most studies focus on the incorporation of ceramic (ZrO_2, TiO_2, SiC) particles with the objective of improving the wear and corrosion resistances of the generated coatings [25-27]. Fewer studies are devoted the incorporation of carbon nanotubes [28-37]. Although the incorporation of those particles undoubtedly modified and sometimes improved the functional properties of the produced PEO coatings, it is not clearly reported to what extend the presence of these dispersed particles into the electrolyte influences the process itself, and more particularly how they may affect the transition from the arc to the "soft" sparking regime. To that regard, this work explores PEO treatments performed with solid particle dispersions and under different processing conditions leading to the appearance of the "soft" sparking regime. More precisely, how different concentrations of carbon nanotubes dispersed in the electrolyte can affect the process and the coatings generated under such conditions. In-situ electrical measurements and optical observations are correlated with the obtained morphology and phase composition of the produced coatings.

2. Materials and methods

PEO treatments were carried out on a 1050 aluminum alloy for which the elemental composition is given in table I. Prior to the PEO treatment, rectangular samples with 25 × 25 × 5 mm^3 in size were ground down to 1200 SiC paper, thoroughly degreased with acetone, ultrasonically rinsed in ethanol and finally dried under warm air.

The carbon nanoparticles dispersed in the electrolyte consist in multi-walled carbon nanotubes Graphistrength C100 (MWCNTs) provided by Arkema, for which the main characteristics are given in table II. They were synthesized by catalytic chemical vapor deposition (CCVD) and remaining impurities consist in residual iron nanoparticles from the synthesis process. They were conditioned as a dry powder of MWCNTs aggregates.

A base solution was prepared by diluting potassium hydroxide (KOH: 1 $g.L^{-1}$ ≅ 18 $mmol.L^{-1}$) and sodium silicate (Na_2SiO_3: 1.65 $g.L^{-1}$ ≅ 13.5 $mmol.L^{-1}$) in deionized water. Its measured electrical conductivity and pH were 7.5 $mS.cm^{-1}$ and 12.6, respectively. From this base solution, different electrolytes were prepared by dispersing MWCNTs in various concentration ranging from 0 to 2.5 $g.L^{-1}$. Finally, and as already described in a previous study [28], carbon-based nanoparticles being intrinsically hydrophobic, a special care was required to properly maintain them dispersed into the electrolyte. Particularly, the electrolyte with the particles was sonicated for 90 min prior to the PEO treatment and a dispersing agent (sodium dodecyl sulfate) was added. Then, to help maintain the dispersion, the PEO treatments were carried out in an ultrasonic bath. To ensure that SDS does not perturb the process, “blank” experiments involving addition of SDS without any CNT were carried out and no significant effect on the electrical signals nor on the transition to the “soft” regime was observed.

PEO treatments were run in a 2 L beaker filled with the prepared electrolytes. The processed aluminum sample was located between two titanium counter-electrodes of 100 × 50 × 1 mm^3 in size. The temperature of the electrolyte was maintained around 50 °C by a copper coil immersed in the beaker and in which 17 °C water circulates. An asymmetrical pulsed bipolar current waveform, provided by a current generator, supplied the electrodes. As depicted in a previous study [28], all the waveform parameters can be adjusted independently over a wide range of values. This allows for designing various signal waveforms by adjusting

the current frequency as well as the charge quantity ratio, defined as the ratio of the anodic to cathodic charge quantity and noted RCQ hereafter. PEO treatments were carried out for two current frequencies (F = 100 and 500 Hz) and two different charge quantity ratios (RCQ = 0.7 and 0.5). The latter were tuned by adjusting the anodic and cathodic period durations while the anodic and the cathodic current amplitudes were maintained at + 8 A and – 8 A, respectively. Process duration was set at 30 min, which was long enough to observe the transition to the "soft" sparking regime for all the processing conditions investigated. After PEO, the treated samples were promptly removed from the electrolyte, thoroughly rinsed with deionized water and cleaned in ethanol in an ultrasonic bath before being dried under a stream of warm air. It is also worth noting that, in order to avoid any possible effect of the electrolyte ageing on the PEO process, a fresh electrolyte was used for each treated sample.

The current and voltage waveforms were regularly recorded using a 1 GHz bandwidth oscilloscope (Agilent Infiniium 54832B). These electrical signals were saved every ten seconds during the first minute of treatment, and then, every minute until the end of the treatment. From these recordings, the evolution of the maximum voltage as a function of the processing time was examined. In addition to the electrical signal recordings, pictures of the samples were periodically taken every 5s during the PEO process in order to observe micro-discharges developing over the processed surface. It is worth noting that only the samples processed without dispersed MWCNTs were subjected to photographs since the electrolyte with dispersed MWCNTs is completely opaque. Regarding the ex situ characterization of the produced PEO coatings, pictures of the overall processed samples were recorded. An image analysis of these pictures was then performed with ImageJ software. To this end, each picture was first converted to gray-scale and binarized. It was then cropped out in order to analyze only a rectangular area of 1.5 cm^2 in the center of the samples. Oxide layers were observed by scanning electron microscopy (Zeiss GeminiSEM 500). Top and cross-sections views of the layers were observed in secondary electron mode (SE) and in back-scattered electron mode

(BSE), respectively. For the latter, and prior to their observations, samples were cut, mounted in resin and gradually polished to achieve a mirror-like surface. Additionally, the phase composition of the oxide coatings was investigated by X-ray diffraction measurements (Bruker D8 Advance) performed in Bragg-Brenato θ/2θ configuration and using the wavelength of the Cu $K_{\alpha 1}$ X-ray emission line (1.5406 Å). The diffractograms were recorded with a step size of 0.02° and a scan range from10 to 100°.

3. Results and discussion

3.1 In situ electrical and optical diagnostic

The evolution of the anodic voltage amplitude during the PEO process for different MWCNTs concentrations is shown in figure 1. Except for the highest concentration in dispersed MWCNTs, all evolutions have a similar trend that is characteristic of a PEO treatment conducted in a current control mode within the specific electrical conditions allowing the "soft" sparking regime to occur [4, 11]. As the process starts, a sharp increase in voltage takes place during the first seconds (~ 50 $V.s^{-1}$) corresponding to the rapid conversion of aluminum into a thin and dense dielectric oxide layer (figure 1.B). When the voltage reaches about 500 V, micro-discharges ignite over the processed surface and the increase rate of anodic potential becomes suddenly much reduced (~ 4 $V.min^{-1}$). This change in the voltage slope is related to the gradual thickening of a porous oxide layer taking place under a micro-discharge regime. Then, at a specific time, depending of the applied conditions, the anodic voltage amplitude starts to decrease which is commonly interpreted as the occurrence of the "soft" sparking regime (figure 1.A).

As a general observation, higher concentrations in MWCNTs result in lower values of the sparking potential. Without dispersed MWCNTs, the sparking potential is about 500 V while it reaches about 430 V with a high MWCNTs concentration of 2 $g.L^{-1}$ (see dotted lines in

figure 1.B). Moreover, it clearly appears that the transition to the “soft” sparking regime takes place earlier for higher concentrations of MWCNTs. Indeed, for the sample processed without MWCNTs, the transition starts after 12 min while it starts after about 1 min for a MWCNTs concentration of 2 $g.L^{-1}$. Depending on the concentration of MWCNTs, figure 1 also evidences that the establishment of the “soft” sparking regime - characterized by the drop in voltage - requires less time as the concentration in MWCNTs gets higher. Indeed, as indicated in figure 1.A, the complete transition last about 6 min without MWCNTs (start at 12 min and end at 18 min) while it only last about 2 min with a concentration of 2 $g.L^{-1}$ (start at 1 min and end at 3 min). Once the “soft” sparking regime is completely established, and until the end of the treatment fixed at 30 min, the anodic voltage amplitude globally remains lower for higher MWCNTs concentrations. Finally, it is also worth noting that for the specific MWCNTs concentration of 2.5 $g.L^{-1}$, the evolution of the anodic voltage amplitude does not exhibit the same trend as for the other concentrations. Indeed, the PEO treatment did not initiate at all. After an initial increase from 0 to 140 V over the first 10 seconds, the voltage gradually decreases and remains at a low value, below 100 V, until the end of the treatment. Although the dispersion of MWCNTs makes the electrolyte completely opaque, the distinctive acoustic emission, inherent to standard PEO treatments remained imperceptible suggesting the absence of micro-discharges over the processed sample.

Aside from the influence of the MWCNTs concentration, figure 2 also puts in evidence the effects of the current frequency and the charge quantity ratio on the evolution of the maximum anodic voltage. Particularly, it appears that the higher the current frequency, the earlier the process switches to the “soft” sparking regime. Indeed, under a charge quantity ratio of 0.7 with a MWCNTs concentration of 1 $g.L^{-1}$, transition starts at about 14 min for a frequency of 100 Hz while it appears earlier at about 8 min for a frequency of 500 Hz. It also appears that increasing the charge quantity ratio from 0.5 to 0.7 results in a delayed transition to “soft” regime. Indeed, under a current frequency of 100 Hz with a MWCNTs concentration

of 1 $g.L^{-1}$, the transition starts at about 7.5 min with a charge quantity ratio of 0.5 while it occurs at about 14 min with a charge quantity ratio of 0.7. Finally, the amplitude of the voltage drop is smaller for a higher RCQ, which is in good agreement with observations reported by Gebarowski *et al.* [11].

As a complement to the evolutions of the anodic voltage amplitude displayed in figures 1 and 2, figure 3 plots the process time at which the "soft" sparking regime occurs as a function of the MWCNTs concentration for the different current frequencies and RCQ values investigated in this work. Whatever the current waveform, it appears that this time linearly decreases as the concentration in MWCNTs increases. This means that the concentration of the dispersed MWCNTs directly influences the PEO process. In addition, the linear regressions of the experimental data points also suggests a threshold in the concentration of the dispersed MWCNTs for which the occurrence of the "soft" sparking regime tends to 0 s and beyond which the PEO process should be inhibited. This was experimentally confirmed with a current frequency of 100 Hz and a charge quantity ratio of 0.5 for which the concentration threshold was expected at 2.25 $g.L^{-1}$. Although the electrolyte was completely opaque, preventing the observation of the sample, the typical crackling sound from the micro-discharges ignition was not emitted suggesting no dielectric breakdown and no oxide was produced on that sample as described below. As shown in figure 1, the maximum anodic voltage amplitude never exceeds 150 V, which is well below the typical breakdown voltage. In addition, figure 3 also confirms that, for a given current pulse frequency, the "soft" sparking regime occurs earlier for a charge quantity ratio of 0.5 compared to 0.7. Moreover, for a given RCQ value, the "soft" sparking regime appears also earlier for a current frequency of 500 Hz compared to 100 Hz.

As mentioned in section 2, for the PEO treatments performed without MWCNTs, it was possible to take pictures of the working electrode, and thus characterized the behavior of the

micro-discharges. By taking pictures periodically along the processing time, the evolution of spatial distribution of micro-discharges over the processed surface was particularly examined. Figure 4 shows successive pictures recorded during PEO treatments conducted with current frequencies of 100 and 500 Hz and with RCQ of 0.5 and 0.7. First of all, whatever the charge quantity ratio, each sequence of pictures shares common features. At the initial stage of the process, just after reaching the sparking potential, micro-discharges randomly ignite all over the processed surface, covering quite homogeneously the sample. After a short processing time (typ. 5 min), micro-discharges ignite preferentially at the corners and at the edges of the samples. This is commonly explained by considering a reinforcement of the intensity of the electric field due to the well-known edge effect [7, 13]. As the transition to the "soft" sparking regime proceeds, depending on the electrical conditions applied, the remaining micro-discharges at the center of the samples gradually self-organize to form localized rings with a diameter between 0.5 mm and 1.3 mm, and with an average diameter of 0.85 mm. These localized rings of micro-discharges are put in evidence by red arrows in figure 4. Nevertheless, figure 4 also shows that for a low RCQ value of 0.5, each ring of micro-discharges persists at the same location with no further evolution while they tend to get wider for a higher RCQ of 0.7. As the process goes on, the micro-discharge rings tend to overlap to form larger areas covered by micro-discharges. Regarding the effect of the frequency on the micro-discharges behavior, figures 4.B and 4.C show that they are much brighter at 100 Hz than those observed at 500 Hz. In addition, although the self-organized rings of micro-discharges remain barely visible over the processed surface at 500 Hz, they also appear more numerous with a smaller size (below 0.6 mm in average diameter) than at 100 Hz frequency (figure 4.C).

3.2 Ex situ characterization of the PEO coatings

Figure 5 shows the macroscopic views of the samples obtained after PEO treatments. From a general point of view, the visual aspect of the samples processed with dispersed MWCNTs

turns darker. As already reported [28], this observation is a first indication of the incorporation of MWCNTs into the PEO coating. Nevertheless, samples exhibit distinctive aspects, depending on both the concentration in dispersed MWCNTs and the applied electrical processing conditions. For the samples treated with the low RCQ value (RCQ = 0.5), signs of embrittlement of the coating around the edges and the corners of the substrate are particularly visible. For some of them, the produced oxide coating locally flakes off revealing the aluminum substrate underneath or a residual oxide sublayer. This embrittlement suggests a poor adhesion of the oxide layer on the substrate. It can be explained by the combination of two concomitant phenomena related to the behavior of the micro-discharges itself directly influenced by the applied electrical conditions. Indeed, on the one hand, the observations concerning the spatial distribution of the micro-discharge evidence that for the samples processed at a low frequency (F = 100 Hz) and a low charge quantity ratio (RCQ = 0.5), micro-discharges are predominantly located at the edges of the sample and repetitively re-ignite at the same locations. Consequently, this cumulative effect of repetitive ignition of micro-discharges promotes the formation of localized and concentrated defects (cracks, high density of pores), which results in the partial embrittlement of the oxide layer. On the other hand, the use of a low RCQ implies a longer cathodic half-period of the current, compared to the anodic one, associated with an abundant reduction of hydrogen cations into hydrogen gas at the substrate / oxide interface, thus promoting delamination of the growing oxide layer [38]. With such a low RCQ, the anodic to cathodic balance is unfavorable to the growth of the coating since the sample mainly acts as a site of cathodic reactions and hydrogen gas formation. In contrast, whatever the concentration in dispersed MWCNTs, the center of the samples processed with the low RCQ of 0.5 are covered by roughly circular spots of about 0.85 mm in diameter giving rise to a leopard-skin appearance. Such an appearance could be explained by considering the collective behavior of the micro-discharges that self-organize into rings after the establishment of the “soft” sparking regime. This is particularly obvious in

figure 6.A that compares the visual aspect of the surface obtained after 30 min (without MWCNTs and at F = 100 Hz and RCQ = 0.5) with the visual aspect of the same sample during its PEO treatment at 30 min. A quite perfect correspondence, in terms of location and size, between the spots of the leopard-skin aspect and the rings of micro-discharges can be drawn. From figure 5, and whatever the concentration of the dispersed MWCNTs, one can also note that with a charge quantity ratio of 0.5 combined with a current pulse frequency of 100 Hz, this leopard-skin aspect is much more pronounced than for higher ratio (RCQ = 0.7) and/or higher frequency (F = 500 Hz). This is explained by considering the fact that under these specific conditions, rings of micro-discharges tend to persist at the same location resulting in a much more spotted surface. Oppositely, with a higher charge quantity ratio of 0.7 or/and a higher current pulse frequency of 500 Hz, these rings of micro-discharges widen after the establishment of the "soft" sparking regime, which favors their coalescence and consequently results in a more homogeneous aspect of the surface.

Regarding the influence of the concentration in dispersed MWCNTs on the final processed surface, figure 5 shows that the leopard-skin aspect changes. A quantitative evaluation of these patterned surfaces was carried out by image analysis and results are reported in figure 6.B. It appears that increasing the concentration in dispersed MWCNTs results in a larger surface coverage by these circular spots. Without MWCNTs, the surface coverage is estimated at about 12 % of the total processed surface while it reaches 61 % for a concentration of 1.5 $g.L^{-1}$. However, the mean diameter of these spots remains relatively equivalent for the different concentrations in MWCNTs (figure 6.B). It means that higher concentrations in dispersed MWCNTs promote the appearance of a larger number of spots of similar dimensions, suggesting therefore that more numerous with similar size rings of micro-discharges developed over the processed surface during the PEO treatment.

Regarding more specifically the samples processed with very high MWCNTs concentrations of 2 $g.L^{-1}$ and 2.5 $g.L^{-1}$, they differentiate themselves from the rest of the other samples (figure 5). For the former sample, large black regions are observed over the surface corresponding to localized high concentrations of aggregated MWCNTs. This can be explained by considering the fact that when using a concentration of MWCNTs greater than 1.5 $g.L^{-1}$ their dispersion in the electrolyte becomes ineffective and unstable, and they tend to reaggregate more easily in the form of large clusters of entangled MWCNTs. For the sample processed with the highest concentration in dispersed MWCNTs (2.5 $g.L^{-1}$), its surface exhibits a shiny metallic aspect close to that of an untreated aluminum substrate. This observation is in good agreement with the associated anodic voltage-time response discussed from figure 1 that evidences that the PEO treatment never started. In addition, and as discussed previously from figure 3, this observation also confirms the existence of a concentration threshold in dispersed MWCNTs above which the PEO process becomes inhibited.

Top-view SEM micrographs displayed in figure 7 show the typical morphologies encountered at different scales on the samples processed without MWCNTs under different electrical conditions. Figure 7.A1, A2 and A3 show the typical surface morphology of the sample processed at 100 Hz with a charge quantity ratio of 0.5. The circular spots are clearly distinguishable from the surrounding surface and they often exhibit large defects at their periphery (figure 7.A1). These defects could result from the localized rings of micro-discharges that formed after the transition to the “soft” sparking regime and that cumulatively damaged the coating at these specific locations due to repetitive ignition of micro-discharges. Spots display a chaotic layout of nodules similar to a “sponge”-like morphology (figure 7.A3) while the surrounding regions show an arrangement of “pancake”-like structures (figure 7.A2). The “sponge”-like morphology is characteristic of a PEO coating grown under the “soft”-sparking regime while the “pancake”-like morphology is commonly observed for PEO

coatings produced within the stronger arc sparking regime [39, 40]. One can specify that the edges of the sample present exclusively the “sponge”-like morphology, similar to the one observed in the spots. When increasing the charge quantity ratio to 0.7, keeping a frequency of 100 Hz, figure 7.B1, B2 and B3 show that the surface morphology consists almost exclusively in the “sponge”-like structure (figure 7.B3). Nevertheless, at few locations, the “pancake”-like structure remains still observable (figure 7.B2). In addition, it appears that there are no huge defects at the interface between the two regions. This could result from the observed widening of the central rings of micro-discharges that gradually progress over the surface. Finally, when increasing both the current pulse frequency at 500 Hz and the charge quantity ratio at 0.7, figure 7.C1, C2 and C3 show, once again, a juxtaposition of “pancake”-like regions (figure 7.C2) with “sponge”-like ones (figure 7.C3), with a larger predominance of the latter. It should be added that at a frequency of 500 Hz, the separation of the two kind of morphologies is not as obvious as shown in figure 7.C1, C2 and C3.

Figure 8 shows cross-section SEM micrographs of the samples processed without MWCNTs under different electrical conditions. At 100 Hz with a RCQ value of 0.5, figure 8.A1, A2 and A3 display the morphological heterogeneities between the spots and the surrounding region. In the spot regions, a thick, porous and damaged oxide layer has grown inward, towards the substrate (figure 8.A3) while only a thin oxide layer, a few micrometers in thickness, is observed in the surrounding regions (figure 8.A2). The morphology inside the spots is highly porous and exhibits large longitudinal cracks in its center and many defects at the interface with the aluminum. Thus, the flaking previously observed on some samples correspond to the large regions where the loosely adherent coating broke off, either directly at the interface with the aluminum or along a crack in the middle of the oxide layer. In contrast, around these spots, the oxide layer is denser but thinner, with a rather good adhesion to the aluminum substrate. This thinner coating results from the early extinction of the micro-discharges in the central region of the sample. In these regions, as the transition to the “soft”

sparking regime proceed, the oxide layer did not continue growing thicker because the micro-discharges gradually extinguished.

By increasing the charge quantity ratio to 0.7 (figure 8.B), the processed surface is covered by a very thick oxide consisting in a porous and irregular outer sublayer and a denser inner sublayer. There is no visible large defect such as cracks nor within the coating nor at the interface with the aluminum. No sign of delamination is observed. These processing conditions appear to be favorable to the generation of a well-adhered thick coating with few defects and an inner sublayer with few micro pores.

For a frequency of 500 Hz and a charge quantity ratio of 0.7 (figure 8.C), the morphology of the coating is very similar to that produced at 100 Hz with the same charge quantity ratio (RCQ = 0.7). It consists in a small porous and irregular outer sub-layer and a denser inner sub-layer. There are no major differences compared to the samples processed at 100 Hz with a charge quantity ratio of 0.7 except for the smaller apparent size of the micro-porosities for the samples processed at 500 Hz.

Interestingly, the sample processed with the highest concentration in dispersed MWCNTs of 2.5 $g.L^{-1}$ (figure 8.D), and for which the PEO treatment never started, the surface does not present any apparent oxide layer but instead a rough metallic surface. Considering that the surface of all samples was polished down to 1200 grit paper prior to each treatment, the observed craters at the surface result from the activated degradation of the metal from the attempted PEO treatment. The absence of audible micro-discharges and the low values of the anodic voltage amplitude (figure 1.A) suggest that the sample was subjected to a bipolar current without ever forming an insulating film on its surface. Indeed the evolution of excessive hydrogen gas formation at the interface between the metal and newly formed oxide could lead to the complete delamination of any oxide formed on the sample. This can explain

the irregularities observed on the surface of the sample that remained in the electrolyte without initiation of the PEO treatment. This mechanism is discussed in detail in section 4.

Figure 9 shows the top-view SEM micrographs of PEO oxide layers grown with various concentrations in dispersed MWCNTs and different charge quantity ratios. Micrographs were taken at the center of the samples where the leopard-skin aspect is mainly observed. Similar morphological features are observed across all MWCNTs concentrations for each RCQ. Indeed, the processing parameters mainly dictate the morphology while increasing concentration in dispersed MWCNTs mainly increase irregularities, especially for a concentration of 2 $g.L^{-1}$ of MWCNTs. Indeed, at this concentration for all processing conditions, some sections of the coating display large protrusions where the coating seems to be much more irregular and thicker than the surrounding area (figure 9.C, F and I).

This observation for samples processed with 2 $g.L^{-1}$ of MWCNTs is even more obvious when looking at the cross-section of the coating. As displayed in figure 10.C, F and I, the coating locally reaches an apparent thickness greater than 200 µm. The coating in those regions consists of a highly porous outer sub-layer, wherein pores can reach up to 15 µm in diameter, on top of a denser inner sub-layer. Often, a large crack is observed, separating the outer porous sub-layer from the inner denser sub-layer.

Overall, the increase in MWCNTs concentration produces thicker yet more porous coatings with more surface irregularities. For concentrations above 1 $g.L^{-1}$, although some regions of the coating display a huge apparent thickness, the number of defects in those regions indicate that the coating seems brittle and the large porosities are generally an indication of poor tribological and corrosion protection capabilities.

As far as the apparent thickness is concerned, figure 11 reports the thickness values from the different samples. For samples with regions of widely different thicknesses, the zones

with greater thickness were used (i.e. spots in the central region of samples processed with a charge ratio of 0.5). Regardless of the processing conditions, the presence of MWCNTs tends to generate thicker coatings compared to standard electrolyte. It should be mentioned that for samples displaying delamination or cracks along the coating, the apparent thickness was corrected by subtracting the size of the crack separating the two sections of the coating in order to give a more relevant estimate of the oxide thickness. Moreover, all samples processed with a RCQ of 0.7 display apparent thickness values greater than those of samples processed with a RCQ of 0.5.

The phase composition of the achieved coatings is summarized in figure 12. For ease of reading, only one diffractogram is displayed as they all reveal the same set of peaks, albeit with different relative intensities. Two allotropic forms of aluminum oxide are detected: the rhombohedral α-Al_2O_3 that corresponds to the stable alumina phase formed at high temperatures (>1100°C) and the cubic η-Al_2O_3 that corresponds to a low temperature metastable phase of alumina. The α-Al_2O_3 is generally more desirable for its superior stability and mechanical properties [41]. As such, the intensity ratio I_α/I_η for the $(113)_\alpha$ and $(400)_\eta$ peaks respectively are usually used to evaluate the relative phase proportion of the two phases. Both peaks are very close without overlapping with other peaks and correspond to similar interplanar distances (2.09 nm and 1.98 nm for $(113)_\alpha$ and $(400)_\eta$ respectively), that is why they are commonly used to evaluate the relative proportion of α to η alumina [42-45]. Regardless of the RCQ or the current frequency, it clearly appears that increasing the concentrations in dispersed MWCNTs leads to a decrease in the α-Al_2O_3 to η-Al_2O_3 intensity ratio, and thus to a decrease in the relative α-Al_2O_3 content in the overall PEO coating. It is also argued here that an early transition to the “soft” sparking regime with a low RCQ value inhibits the formation of the α-Al_2O_3 phase. Indeed, figure 12.B and C point out that a higher RCQ value is much more beneficial to the growth of the α-Al_2O_3 phase. Both observations are latter discussed in section 4.

4. Discussion

In regard to the influence of the MWCNTs on the PEO process and more specifically on the transition to the "soft" sparking regime, the characterization of the generated coatings points out that the average growth rate of the alumina layer increases with the concentration in MWCNTs in the electrolyte, which indicates an accelerated growth kinetics. Moreover, previous work with electrical conditions that did not typically lead to the "soft" sparking regime also evidence that the presence of MWCNTs in the electrolyte leads to the formation of thicker oxide coating for equal treatment duration [28]. In addition, the growth kinetics is accelerated whatever the current frequency or RCQ value. In parallel, it is observed that the transition to the "soft" regime is also linearly correlated with the concentration in MWCNTs. As the concentration of MWCNTs increases, the duration necessary to reach the transition to the "soft" sparking regime decreases. As pointed out by Matykina *et al.* [15, 46], for a given set of electrical parameters, the transition to the "soft" sparking regime is initiated once a sufficiently thick oxide layer is formed on the surface of the sample. They proposed a two-step process wherein a first oxide layer is formed by conventional anodizing in sulfuric acid before subjecting the sample to a PEO treatment under "soft" sparking conditions. When an anodic film of sufficient thickness was formed during the pre-anodizing step, the transition to the "soft" regime during the PEO treatment would occur after less than a minute while for thinner anodic films, the transition would occur later in the PEO treatment. In regards to PEO treatments with MWCNTs, the increased oxide growth kinetics can thus explain both the fact that the transition occurs earlier and the fact that the transition itself is faster. Indeed, as the oxide growth kinetics is increased, the necessary oxide thickness to initiate the transition is attained earlier thus inducing an earlier transition to the "soft" sparking regime. The faster oxide growth kinetics is maintained after the transition, especially for treatments with RCQ = 0.7 as the final thickness of the film increases noticeably with the concentration of MWCNTs.

Regarding the inhibition of the PEO treatment for very high concentrations of MWCNTs (> 2.25 $g.L^{-1}$ in the present study) and low RCQ of 0.5, several factors have to be considered. First, as shown from the heterogeneous morphology and the delamination of the oxide layers formed for lower concentrations of MWCNTs, those electrical conditions are not favorable to the formation of a PEO oxide. Moreover, numerous defects are observed at the interface between the oxide and the aluminum substrate. Knowing that, during the very first moments of the treatment, before the appearance of micro-discharges, the aluminum sample experiences anodization under high current and voltages. In this first stage, it is crucial that an insulating aluminum oxide film rapidly develops over the whole surface of the sample. Ishino *et al.* [47] and Takahashi *et al.* [48], studied the anodization of aluminum under AC conditions. They demonstrated that if the barrier anodic film does not properly cover the surface of the aluminum (too many defects), hydrogen cations will migrate towards the oxide/aluminum interface during the cathodic polarization and cause the delamination of the film by mechanical stress from the formation of hydrogen gas. This is of great importance when working with low RCQ values since there is a strong predominance of the cathodic current relative to the anodic one. Second, the presence of electrically conductive MWCNTs in too high concentration could prevent the formation of an insulating film over the whole surface of the sample, which would explain why the anodic voltage amplitude never reaches values above 120 V. Without the insulating film covering the whole surface, combined with the evolution of hydrogen gas at the oxide/aluminum interface delaminating parts of the oxide, the sample is never fully insulated by an oxide film covering the whole surface, the breakdown potential is never reached and no micro-discharge can ignite, thus prohibiting the initiation of the PEO treatment. Similar observations were made by Shimabukuro *et al.* concerning the PEO treatment of titanium in electrolytes containing Ag^{+} ions [49, 50]. They observed that for concentrations in Ag^{+} ions exceeding 10 mM, the voltage never reached values above 120 V and no oxide coating would generate on the metallic substrate. This was

attributed to the absence of an insulating layer, thus preventing the initiation of the PEO treatment.

Regarding the phase composition of the oxide, a higher RCQ value (RCQ = 0.7 compared to 0.5) leads to a higher proportion of α-Al_2O_3. This can be explained from the fact that for low RCQ values (0.5), the micro-discharges completely disappear from a major section of the sample's surface. This contributes to reducing the heat generated within the coating and thus inhibits the transition from η to α alumina that can occur at temperatures in the range of 1050 to 1200 °C [51]. Moreover, the morphology of the coating plays an important role: heat accumulation is predominant in the middle of the coating, far from both the electrolyte and the aluminum substrate that both act as efficient heat sinks. For the lower charge quantity ratios (RCQ = 0.5), the coatings are porous throughout their whole thickness and allow a deeper infiltration of the electrolyte that will quench the newly formed oxide and prevent heat buildup. On the contrary, coatings formed with a higher charge quantity ratio (RCQ = 0.7) present a dense inner sublayer where heat generated from the micro-discharges and resistive behavior of the coating cannot be efficiently evacuated either by the electrolyte or through the metallic substrate. The formation of α-Al_2O_3 thus preferentially takes place in the central region of the dense inner layer where heat buildup is the most pronounced [52-54]. Regarding the decrease in α-Al_2O_3 relative to η-Al_2O_3 for higher concentrations of MWCNTs, it can be explained by several factors. First, the overall anodic voltage amplitude is lower over the treatment duration for higher concentrations of MWCNTs, thus generating less heat from the resistive elements of the electrolytic system and as such inhibiting the formation of the high-temperature phase alumina α-Al_2O_3. Second, the MWCNTs having excellent thermal conductivity, their incorporation in the oxide can enhance the evacuation of the heat generated within the coating, once again preventing the formation of the high temperature phase. Third, the increased porosity, especially in the outer porous sublayer in contact with the electrolyte improves heat evacuation from the quenching effect of the electrolyte infiltrating the coating

through the large network of pores. The combination of all these factors leads to a decrease in the proportion of α-Al_2O_3 relative to η-Al_2O_3 for higher concentrations of MWCNTs.

5. Conclusion

PEO treatments under electrical conditions leading to the appearance of the "soft" sparking regime in various concentrations of dispersed MWCNTs showed that the transition to the "soft" sparking occurs earlier for higher concentrations of MWCNTs. More precisely, the time at which this transition initiates decreases linearly with the increase in MWCNTs concentration. This is largely attributed to an increased growth kinetics given that the resulting coating thickness increases linearly with the concentration of MWCNTs. As such, for adequate electrical conditions, the addition of MWCNTs leads to the formation of thicker oxides while reducing energy consumption. However, the benefits from this early transition to the soft regime are mitigated by the fact that coatings formed in MWCNTs dispersions exhibit a higher porosity as the concentration of MWCNTs increases. Moreover, regarding the phase composition of the oxide, the increase in MWCNTs concentration leads to a decrease in α-Al_2O_3 due to less heat generation from lower anodic voltages and better heat evacuation from the highly conductive MWCNTs incorporated in the coating, thus preventing heat accumulation within the oxide. Although the "soft" sparking regime is usually beneficial to improving the density and phase composition of PEO coatings, a too early transition to the "soft" sparking regime due to the addition of excessive amounts of MWCNTs (2 $g.L^{-1}$) leads to the formation of highly irregular and porous coatings with numerous defects. Regarding the charge quantity ratio, similar conclusions can be made. Although the lower value (RCQ = 0.5) leads to faster transition to the "soft" sparking regime, the generated coatings are highly heterogeneous since coating growth stops on a large section of the sample. The excessive unbalance between the cathodic and anodic current is unfavorable to the formation of dense and homogeneous coatings. To conclude, in the present study, the best coatings were

generated for charge quantity ratios closer to 1 (RCQ = 0.7) and intermediate concentrations of MWCNTs (1 $g.L^{-1}$) leading to an increase in coating thickness without introducing defects or excessive porosity.

Author Contributions

C. Da Silva Tousch : Conceptualization, Methodology, Investigation, Writing – Original Draft, Visualization

L. Magniez : Investigation, Writing – Review & Editing

S. Fontana : Supervision

G. Marcos : Writing – Review & Editing' Supervision

C. Hérold : Supervision

G. Henrion : Conceptualization, Writing – Review & Editing, Supervision, Project administration, Funding acquisition

T. Czerwiec : Conceptualization, Writing – Review & Editing, Supervision, Project administration, Funding acquisition

J. Martin : Conceptualization, Writing – Review & Editing, Visualization, Supervision, Project administration, Funding acquisition

Acknowledgments

This work was supported by the French Government through the program “Investissements d’avenir” operated by the French National Research Agency (ANR) and referenced to as ANR-11-LABX-0008-01 (‘Labex DAMAS’) along with the support from the Conseil Régional de la Région Grand Est for granting C. Da Silva Tousch’s PhD work under decision 19_GE_049.

The author would also like to thank the French national research agency (ANR) for granting L. Magniez PhD under project Camfre (ANR21-CE08-00029).

The authors would also like to acknowledge contributions from the following :

- The competence cluster on metallography and electron microscopy (CC-3M) at Institut Jean Lamour.
- The competence cluster on diffraction, diffusion, fluorescence and tomography (CC-Xγ) at Institut Jean Lamour.

List of references

[1] A.L. Yerokhin, X. Nie, A. Leyland, A. Matthews, S.J. Dowey, Plasma electrolysis for surface engineering, Surf. Coat. Technol. 122 (1999) 73–93.

[2] T.W. Clyne, S.C. Troughton, A review of recent work on discharge characteristics during plasma electrolytic oxidation of various metals, Int. Mater. Rev. 64 (2019) 127-162.

[3] S.C. Troughton, A. Nominé, J. Dean, T.W. Clyne, Effect of individual discharge cascades on the microstructure of plasma electrolytic oxidation coatings, Appl. Surf. Sci. 389 (2016) 260–269.

[4] F. Jaspard-Mécuson, T. Czerwiec, G. Henrion, T. Belmonte, L. Dujardin, A. Viola, J. Beauvir, Tailored aluminium oxide layers by bipolar current adjustment in the plasma electrolytic oxidation (PEO) process. Surf. Coat. Technol. 201 (2007) 8677–8682.

[5] Q.P. Tran, Y.C. Kuo, J.K. Sun, J.L. He, T.S. Chin, High quality oxide-layers on Al-alloy by micro-arc oxidation using hybrid voltages, Surf. Coat. Technol. 303 (2016) 61-67.

[6] P. Hermanns; S. Boeddeker; V. Bracht; N. Bibinov; P. Awakowicz, In-situ control of microdischarge characteristics in unipolar pulsed plasma electrolytic oxidation of aluminum, J. Phys. D. 53 (2020) 43.

[7] J. Martin, A. Melhem, I. Shchedrina, T. Duchanoy, A. Nominé, G. Henrion, T. Czerwiec, T. Belmonte, Effects of electrical parameters on plasma electrolytic oxidation of aluminium, Surf. Coat. Technol. 221 (2013) 70–76.

[8] J. Martin, A. Nominé, J. Brochard, J.L. Briançon, C. Noël, T. Belmonte, T. Czerwiec, G. Henrion, Delay in micro-discharges appearance during PEO of Al: Evidence of a mechanism of charge accumulation at the electrolyte/oxide interface, Appl. Surf. Sci. 410 (2017) 29-41.

[9] S. Song, B. Chen, H. Li, R. Shi, C. Liu, B. Yang, G.F. de la Fuente, Growth behavior and insulation property of the oxide layer during micro-arc oxidation of aluminium in “soft” regime condition, J. Mater. Sci. 58 (2023 7136-7148.

[10] E. Matykina, R. Arrabal, D.J. Scurr, A. Baron, P. Skeldon, G.E. Thompson, Investigation of the mechanism of plasma electrolytic oxidation of aluminium using 18-O tracer, Corros. Sci. 52 (2010) 1070–1076.

[11] W. Gebarowski, S. Pietrzyk, Influence of the cathodic pulse on the formation and morphology of oxide coatings on aluminium produced by plasma electrolytic oxidation, Arch. Metall. Mater. 58 (2013) 241–245.

[12] D.S. Tsai, C.C. Chou, Review of the Soft Sparking Issues in Plasma Electrolytic Oxidation, Metals 8 (2018) 105.

[13] A. Melhem, G. Henrion, T. Czerwiec, J.L. Briançon, T. Duchanoy, F. Brochard, T. Belmonte, Changes induced by process parameters in oxide layers grown by the PEO process on Al alloys, Surf. Coat. Technol. 205 (2011) S133-S136.

[14] A.B. Rogov, A. Yerokhin, A. Matthews, The role of cathodic current in plasma electrolytic oxidation of aluminum: phenomenological concepts of the“soft sparking”mode, Langmuir 33 (2017) 11059–11069.

[15] E. Matykina, R. Arrabal, P. Skeldon, G.E. Thompson, P. Belenguer, AC PEO of aluminium with porous alumina precursor films, Surf. Coat. Technol. 205 (2010) 1668–1678.

[16] M.P. Kamil, M. Kaseem, Y.G. Ko, Soft plasma electrolysis with complex ions for optimizing electrochemical performance, Sci. Rep. 7 (2017) 4458.

[17] R. Arrabal, E. Matykina, T. Hashimoto, P. Skeldon, G.E. Thompson, Characterization of AC PEO coatings on magnesium alloys, Surf. Coat. Technol. 203 (2009) 2207–2220.

[18] F. Tjiang, L.W. Ye, Y.J. Huang, C.C. Chou, D.S. Tsai, Effect of processing parameters on soft regime behavior of plasma electrolytic oxidation of magnesium, Ceram. Int. 43 (2017) S567–SS72.

[19] Q. Tang, T. Qiu, P. Ni, D. Zhai, J. Shen, Soft sparking discharge mechanism of micro-arc oxidation occurring on titanium alloys in different electrolytes, Coatings 12 (2022) 1191.

[20] Y.L. Cheng, J.H. Cao, Z.M. Peng, Q. Wang, E. Matykina, P. Skeldon, G.E. Thompson, Wear-resistant coatings formed on Zircaloy-2 by plasma electrolytic oxidation in sodium aluminate electrolytes, Electrochim. Acta. 116 (2014) 453–466.

[21] Y.L. Cheng, T. Wang, S.X. Li, Y. Cheng, J. Cao, H. Xie, The effects of anion deposition and negative pulse on the behaviours of plasma electrolytic oxidation (PEO)-a systematic study of the PEO of a zirlo alloy in aluminate electrolytes, Electrochim. Acta. 225 (2017) 47–68.

[22] J. Martin, P. Leone, A. Nomine, D. Veys-Renaux, G. Henrion, T. Belmonte, Influence of electrolyte ageing on the plasma electrolytic oxidation of aluminium, Surf. Coat. Technol. 269 (2015) 36–46.

[23] X. Lu, M. Mohedano, C. Blawert, E. Matykina, R. Arrabal, K.U. Kainer, M.L. Zheludkevich, Plasma electrolytic oxidation coatings with particle additions – A review, Surf. Coat. Technol. 307 (2016) 1165-1182.

[24] M. O’Hara, S.C. Troughton, R. Francis, T.W. Clyne, The incorporation of particles suspended in the electrolyte into plasma electrolytic oxidation coatings on Ti and Al substrates, Surf. Coat. Technol. 385 (2020) 125354.

[25] A. Bahramian, K. Raeissi, A. Hakimizad, An investigation of the characteristics of Al_2O_3/TiO_2 PEO nanocomposite coating, Appl. Surf. Sci. 351 (2015) 13-26.

[26] X. Lu, C. Blawert, Y. Huang, H. Ovri, M.L. Zheludkevich, K.U. Kainer, Plasma electrolytic oxidation coatings on Mg alloy with addition of SiO_2 particles, Electrochim. Acta. 187 (2016) 20-33.

[27] K.M. Lee, B.U. Lee, Y.S. Il, E.S. Lee, B. Yoo, D.H. Shin, Evaluation of plasma temperature during plasma oxidation processing of AZ91 Mg alloy through analysis of the melting behavior of incorporated particles, Electrochim. Acta. 67 (2012) 6-11.

[28] C. Da Silva Tousch, J. Martin, G. Marcos, T. Czerwiec, G. Henrion, Evidence of in-depth incorporation of carbon nanotubes in alumina layers grown by plasma electrolytic oxidation, Surf. Coat. Technol. 440 (2022) 128489.

[29] K.M. Lee, Y.G. Ko, D.H. Shin, Incorporation of multi-walled carbon nanotubes into the oxide layer on a 7075 Al alloy coated by plasma electrolytic oxidation: coating structure and corrosion properties, Curr. Appl. Phys. 11 (2011) 55-59.

[30] K.M. Lee, Y.G. Ko, D.H. Shina, Incorporation of carbon nanotubes into micro-coatings film formed on aluminum alloy via plasma electrolytic oxidation, Mater. Lett. 65 (2011) 2269-2273.

[31] Y.S. Kim, H.W. Yang, K.R. Shin, Y.G. Ko, D.H. Shin, Heat dissipation properties of oxide layers formed on 7075 Al alloy via plasma electrolytic oxidation, Surf. Coat. Technol. 269 (2015) 114-118.

[32] Y. Yürektürk, F. Muhaffel, M. Baydogan, Characterization of micro arc oxidized 6082 aluminum alloy in an electrolyte containing carbon nanotubes, Surf. Coat. Technol. 269 (2015) 83-90.

[33] M. Sabouri, S.M. Mousavi Khoei, Plasma electrolytic oxidation in the presence of multiwall carbon nanotubes on aluminum substrate: Morphological and corrosion studies, Surf. Coat. Technol. 334 (2018) 543-555.

[34] M. Hwang, W. Chung, Effects of a Carbon Nanotube Additive on the Corrosion-Resistance and Heat-Dissipation Properties of Plasma Electrolytic Oxidation on AZ31 Magnesium Alloy, Mater. 11 (2018) 2438.

[35] L. Yu, P. Jia, Y. Song, B. Zhao, Y. Pan, J. Wang, H. Cui, R. Feng, H. Li, X. Cui, Z. Gao, X. Fang, L. Zhang, Effect of carbon nanotubes on the microstructure and properties of plasma electrolytic oxidized ceramic coatings on high silicon aluminum alloy, J. Mater. Res. Technol. 18 (2022) 3541-3552.

[36] Y. Guo, L. Xu, J. Luan, Y. Wan, R. Liac, Effect of carbon nanotubes additive on tribocorrosion performance of micro-arc oxidized coatings on Ti6Al4V alloy, Surf. Interfaces. 28 (2022) 101626.

[37] R. Kara, H. Zengin, Tribological and Electrochemical Corrosion Properties of CNT-Incorporated Plasma Electrolytic Oxidation (PEO) Coatings on AZ80 Magnesium Alloy, Acta Metall. Sin. 35 (2022) 1195–1206.

[38] A. Gasco Owens, D. Veys-Renaux, E. Rocca, Reverse scan polarization of anodic aluminum oxide until detachment in sulfuric acid: Mechanisms and morphologies, Electrochim. Acta, 435 (2022) 141361.

[39] R.O. Hussein; X. Nie, D. O Northwood, A. Yerokhin, A. Matthews, Spectroscopic study of electrolytic plasma and discharging behaviour during the plasma electrolytic oxidation (PEO) process. J. Phys. D Appl. Phys. 43 (2010) 105203.

[40] S.G. Moga, D.A. Negrea, C.M. Ducu, V. Malinovschi, A.G. Schiopu, E. Coaca, I. Patrascu, The Influence of Processing Time on Morphology, Structure and Functional Properties of PEO Coatings on AZ63 Magnesium Alloy. Appl. Sci. 12 (2022) 12848.

[41] J. Tian, Z. Luo, S. Qi, X. Sun, Structure and antiwear behavior of micro-arc oxidized coatings on aluminum alloy, Surf. Coat. Technol. 154 (2002) 1-7.

[42] C.H. Hsu, H.P. Teng, F.H. Lu, Effects of addition of $Al(NO_3)_3$ to electrolytes on alumina coatings by plasma electrolytic oxidation, Surf. Coat. Technol., 205 (2011) 3677-3682.

[43] H. Wu, J. Wang, B. Long, B. Long, Z. Jin, W. Naidan, F. Yu, D. Bi, Ultra-hard ceramic coatings fabricated through microarc oxidation on aluminium alloy, Appl. Surf. Sci., 252 (2005) 1545-1552.

[44] R.H.U. Khan, A. Yerokhin, X. Li, H. Dong, A. Matthews, Surface characterisation of DC plasma electrolytic oxidation treated 6082 aluminium alloy: Effect of current density and electrolyte concentration, Surf. Coat. Technol., 205 (2010) 1679-1688.

[45] V. Dehnavi, X.Y. Liu, B.L. Luan, D.W. Shoesmith, S. Rohani, Phase transformation in plasma electrolytic oxidation coatings on 6061 aluminum alloy, Surf. Coat. Technol. 251 (2014) 106-114.

[46] E. Matykina, R. Arrabal, A. Mohamed, P. Skeldon, G.E. Thompson, Plasma electrolytic oxidation of pre-anodized aluminium, Corros. Sci. 51 (2009) 2897-2905.

[47] M. Ishino, H. Hashimoto, H. Asoh, Effect of Cathodic Current on the Structural Features of Oxide Films formed by AC Anodization of Aluminum, J. Electrochem. Soc. 164 (2017) 939.

[48] H. Takahashi, K. Kasahara, K. Fujiwara, M. Seo, The cathodic polarization of aluminum covered with anodic oxide films in a neutral borate solution—I. The mechanism of rectification, Corros. Sci. 36 (1994) 677.

[49] M. Shimabukuro, Y. Tsutsumi, R. Yamada, M. Ashida, P. Chen, H. Doi, K. Nozaki, A. Nagai, T. Hanawa, Investigation of realizing both antibacterial property and osteogenic cell compatibility on titanium surface by simple electrochemical treatment, ACS Biomater. Sci. Eng. 5 (2019) 5623–5630.

[50] M. Shimabukuro, H. Tsutsumi, Y. Tsutsumi, T. Manaka, P. Chen, M. Ashida, K. Ishikawa, H. Katayama, T. Hanawa, Enhancement of antibacterial property of titanium by two-step micro arc oxidation treatment, Dent. Mater. J. 40 (2021) 592–598.

[51] C.J.P. Steiner, D.P.H. Hasselman, R.M. Spriggs, Kinetics of the gamma-to-alpha alumina phase transformation, J. Am. Ceram. Soc. 54 (1971) 412-413.

[52] F. Simchen, R. Morgenstern, S. Clauß, T. Mehner, T. Lampke, Dissolution Behavior of Different Alumina Phases within Plasma Electrolytic Oxidation Coatings, Coatings. 12 (2021) 1205.

[53] X. Huang, L. Famiyeh. Plasma Electrolytic Oxidation Coatings on Aluminum Alloys: Microstructures, Properties, and Applications, Mod. Concept. Material. Sci. 2 (2019). MCMS.MS.ID.000526.

[54] M. Sieber, F. Simchen, R. Morgenstern, I. Scharf, T. Lampke, Plasma electrolytic oxidation of high-strength aluminum alloys-substrate effect on wear and corrosion performance, Metals. 5 (2018) 1-17.

List of tables

Table I: Elemental composition of the 1050 aluminum substrate.

Element	Fe, Ti, Zn	Si	Cu	Mg	Mn	Al
wt.%	< 0.5	< 0.25	0.05	< 0.05	< 0.05	Balance

Table II: Initial characteristics of the multi-walled carbon nanotubes (MWCNTs). SEM[1], TEM[2] and TGA[3] stand for scanning electron microscopy, transmission electron microscopy, and thermogravimetric analysis, respectively.

Aggregate dimensions[1]	Purity[3]	Diameter[2]	Length[1,3]
200 – 1000 µm	93 wt.%	12 - 20 nm	0.1 – 10 µm

List of figures

Figure 11: Scatter interval of the PEO coating thickness for 30 random measurement points as a function of the concentration in dispersed MWCNTs for the different electrical conditions applied (F = 100 and 500 Hz ; RCQ = 0.5 and 0.7). Bars indicate the average, first and third quartiles for each point distribution.

Figure 12: Summary of the X-ray diffraction results showing (A) the representative diffractograms with peak indexation collected with different MWCNTs concentrations, different current pulse frequencies and different charge quantity ratio, (B) an inset view of the α-Al_2O_3 (113) and η-Al_2O_3 (400) peaks, and (C) the intensity ratios of the α-Al_2O_3 (113) and η-Al_2O_3 (400) peaks calculated for each processed sample.

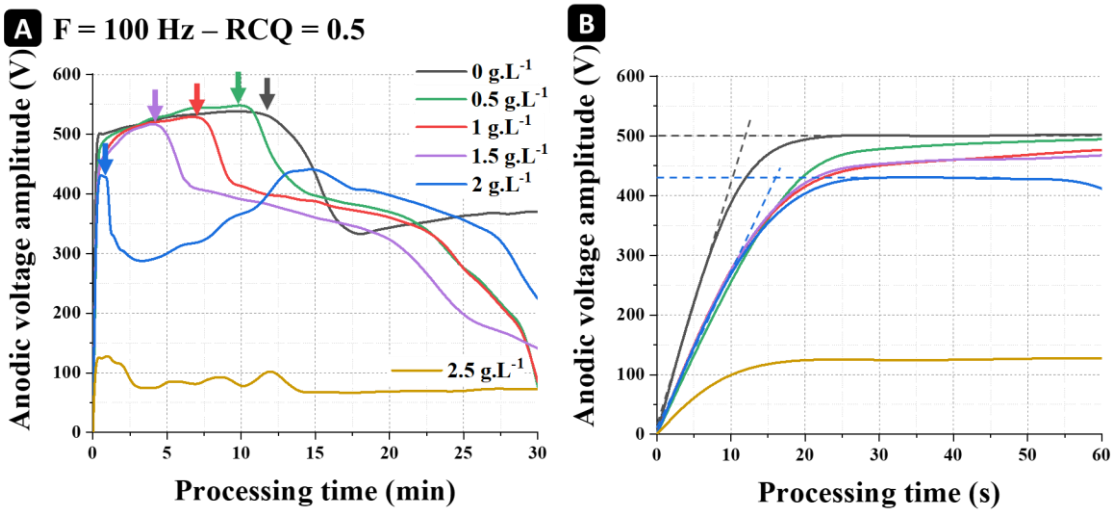
A
F = 100 Hz – RCQ = 0.5
Anodic voltage amplitude (V)
Processing time (min)
0 g.L-1
0.5 g.L-1
1 g.L-1
1.5 g.L-1
2 g.L-1
2.5 g.L-1
B
Anodic voltage amplitude (V)
Processing time (s)

1

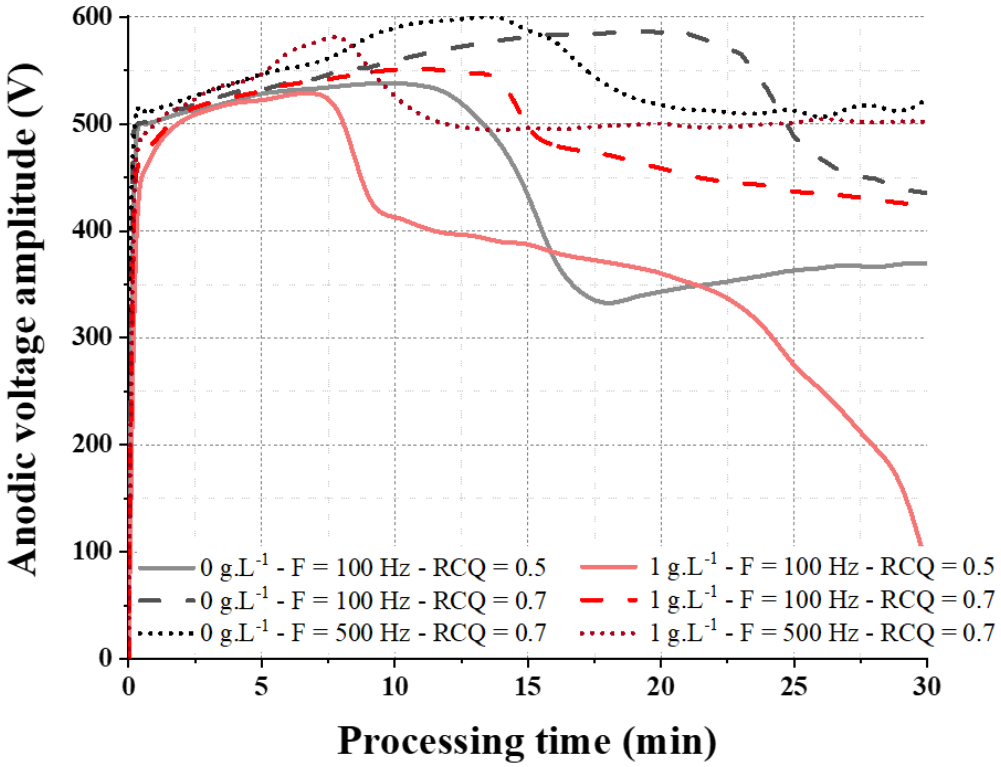
Anodic voltage amplitude (V)
Processing time (min)
0
100
200
300
400
500
600
0
5
10
15
20
25
30
0 g.L-1 - F = 100 Hz - RCQ = 0.5
0 g.L-1 - F = 100 Hz - RCQ = 0.7
0 g.L-1 - F = 500 Hz - RCQ = 0.7
1 g.L-1 - F = 100 Hz - RCQ = 0.5
1 g.L-1 - F = 100 Hz - RCQ = 0.7
1 g.L-1 - F = 500 Hz - RCQ = 0.7

2

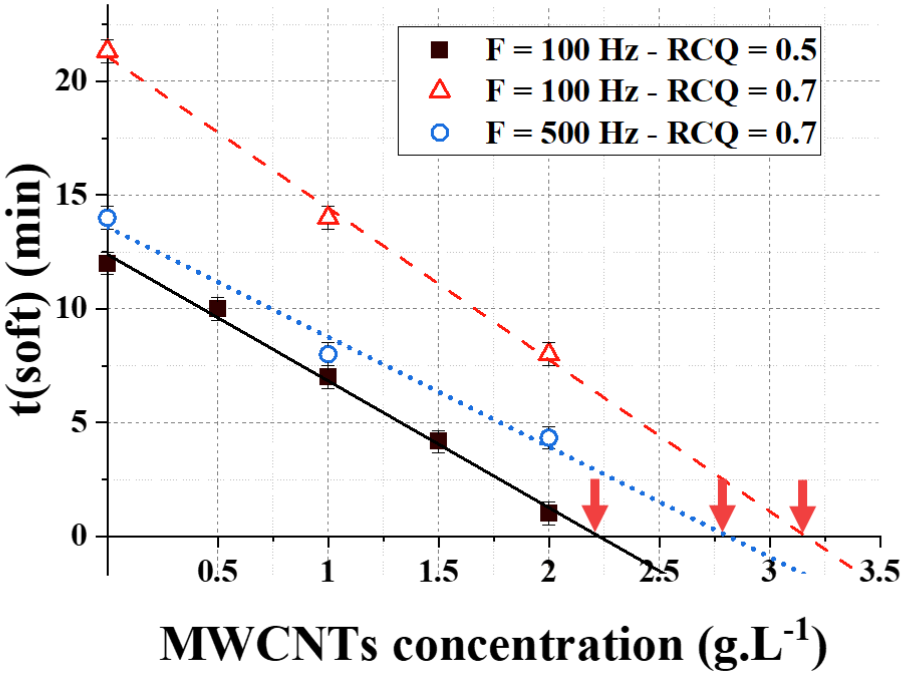
F = 100 Hz - RCQ = 0.5
F = 100 Hz - RCQ = 0.7
F = 500 Hz - RCQ = 0.7
t(soft) (min)
0
5
10
15
20
0.5
1
1.5
2
2.5
3
3.5
MWCNTs concentration (g.L-1)

3

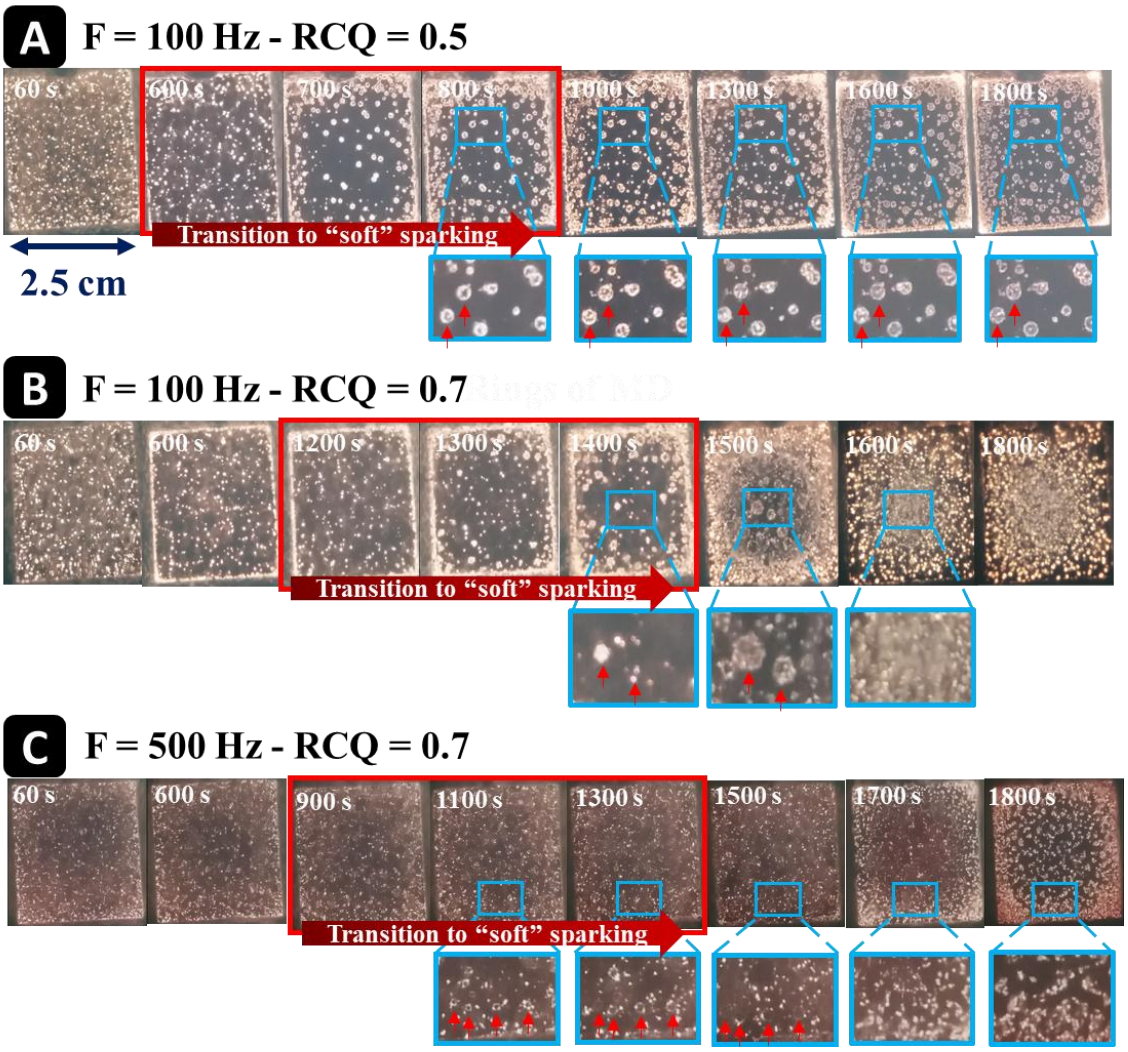
A
F = 100 Hz - RCQ = 0.5
60 s
600 s
700 s
800 s
1000 s
1300 s
1600 s
1800 s
Transition to "soft" sparking
2.5 cm
B
F = 100 Hz - RCQ = 0.7
60 s
600 s
1200 s
1300 s
1400 s
1500 s
1600 s
1800 s
Transition to "soft" sparking
C
F = 500 Hz - RCQ = 0.7
60 s
600 s
900 s
1100 s
1300 s
1500 s
1700 s
1800 s
Transition to "soft" sparking

4

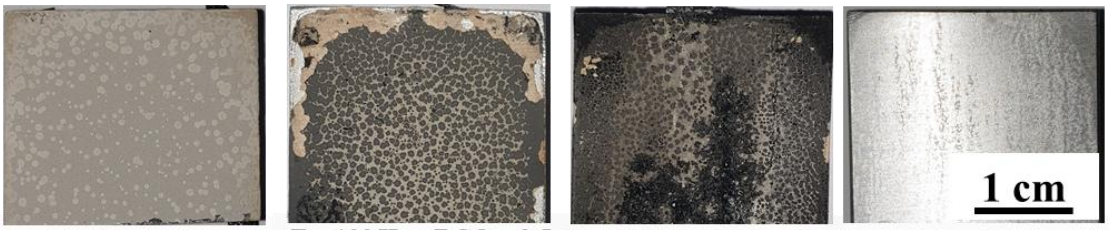

F = 100 Hz – RCQ = 0.5
0 g.L^{-1}

F = 100 Hz – RCQ = 0.5
1 g.L^{-1}

F = 100 Hz – RCQ = 0.5
2 g.L^{-1}

F = 100 Hz – RCQ = 0.5
2.5 g.L^{-1}

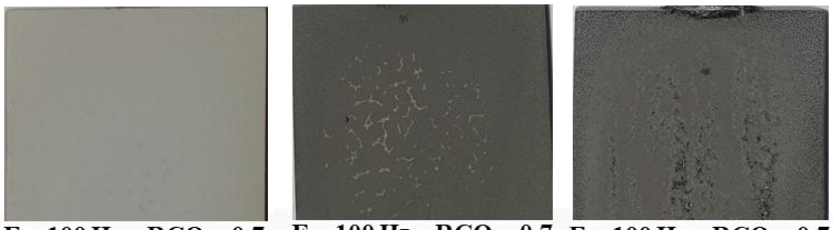

F = 100 Hz – RCQ = 0.7
0 g.L^{-1}

F = 100 Hz – RCQ = 0.7
1 g.L^{-1}

F = 100 Hz – RCQ = 0.7
2 g.L^{-1}

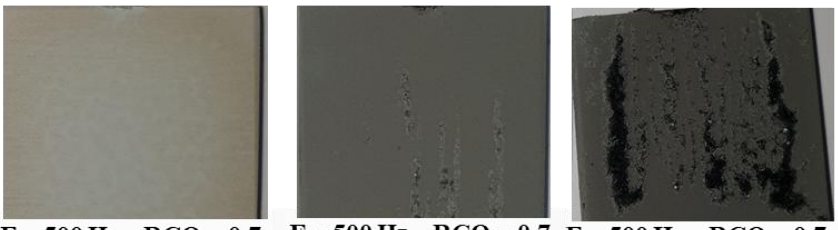

F = 500 Hz – RCQ = 0.7
0 g.L^{-1}

F = 500 Hz – RCQ = 0.7
1 g.L^{-1}

F = 500 Hz – RCQ = 0.7
2 g.L^{-1}

5

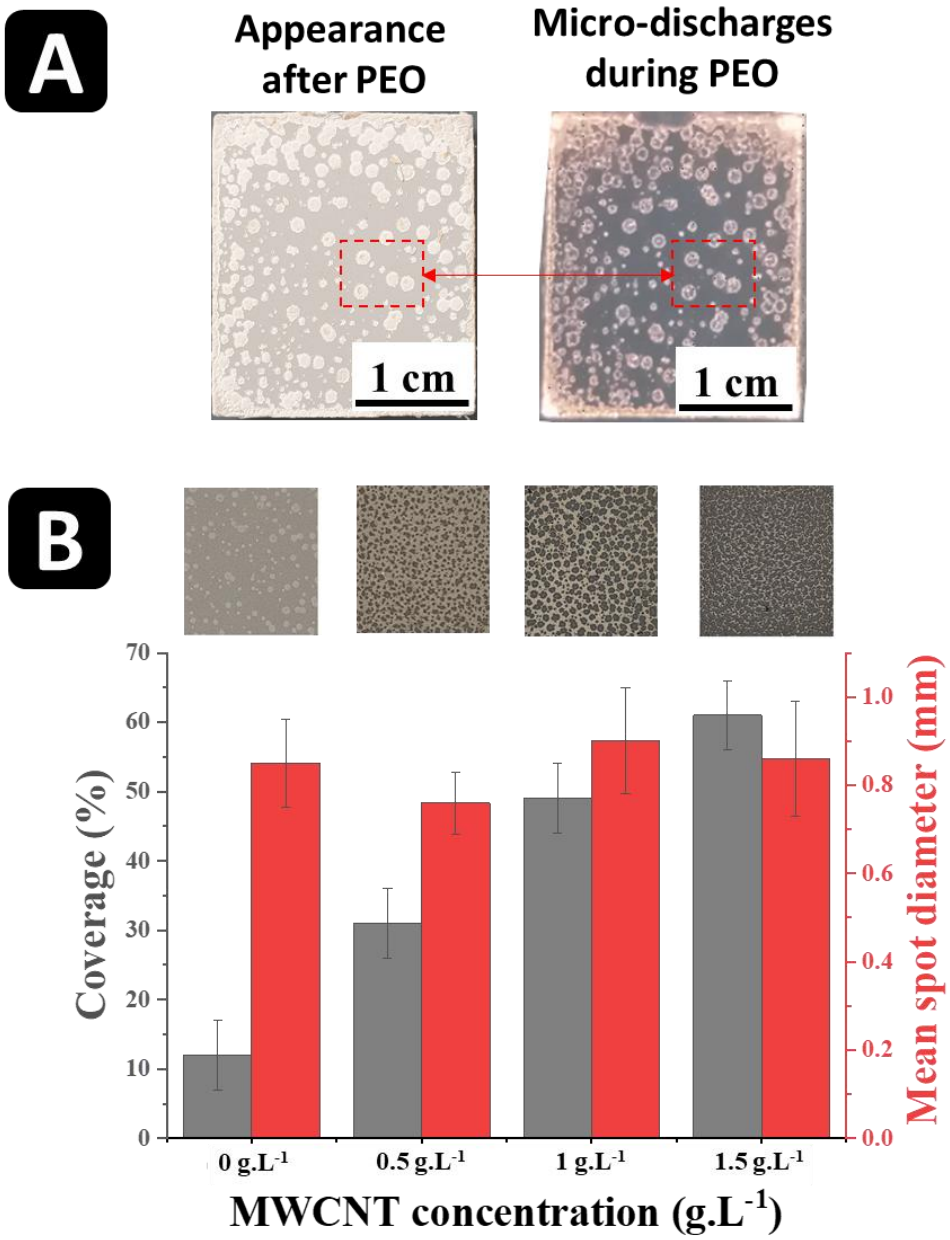
A
Appearance after PEO
Micro-discharges during PEO
1 cm
1 cm
B
Coverage (%)
Mean spot diameter (mm)
0 g.L-1
0.5 g.L-1
1 g.L-1
1.5 g.L-1
MWCNT concentration (g.L-1)

6

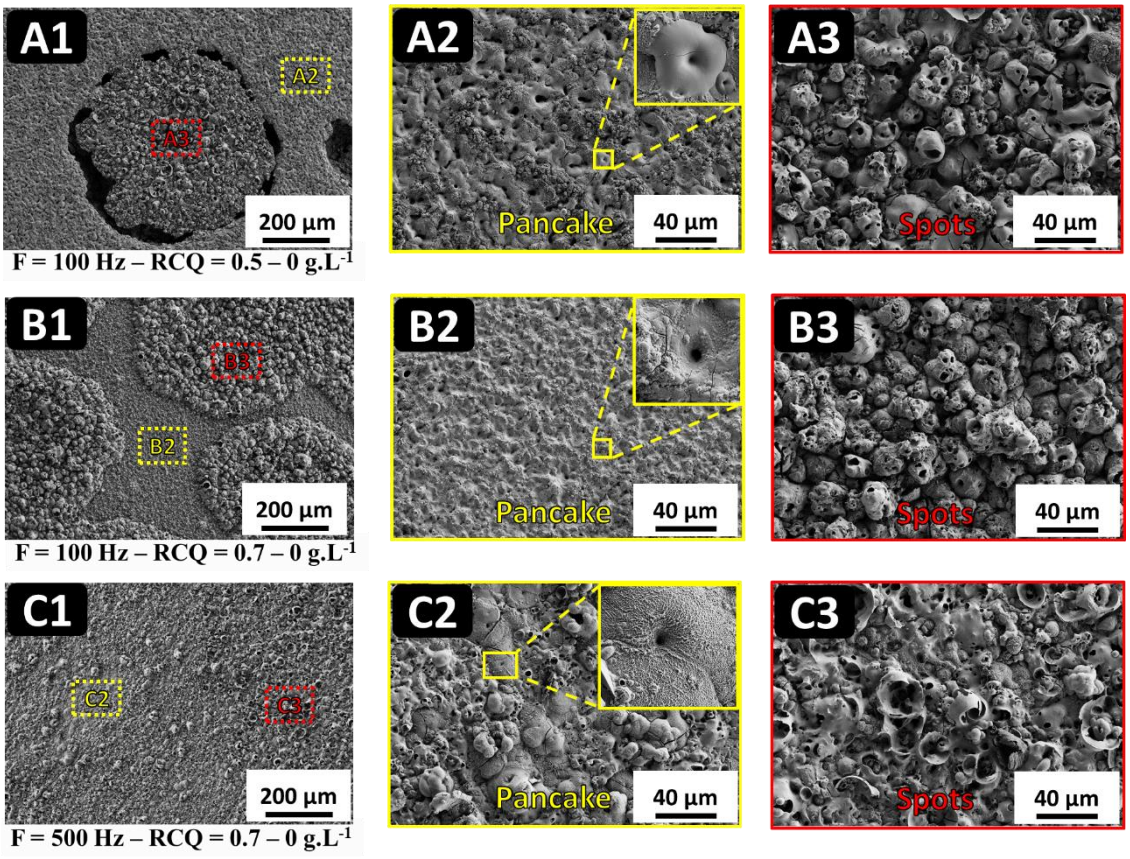
A1
A2
A3
200 µm
F = 100 Hz – RCQ = 0.5 – 0 g.L-1
A2
Pancake
40 µm
A3
Spots
40 µm
B1
B3
B2
200 µm
F = 100 Hz – RCQ = 0.7 – 0 g.L-1
B2
Pancake
40 µm
B3
Spots
40 µm
C1
C2
C3
200 µm
F = 500 Hz – RCQ = 0.7 – 0 g.L-1
C2
Pancake
40 µm
C3
Spots
40 µm

7

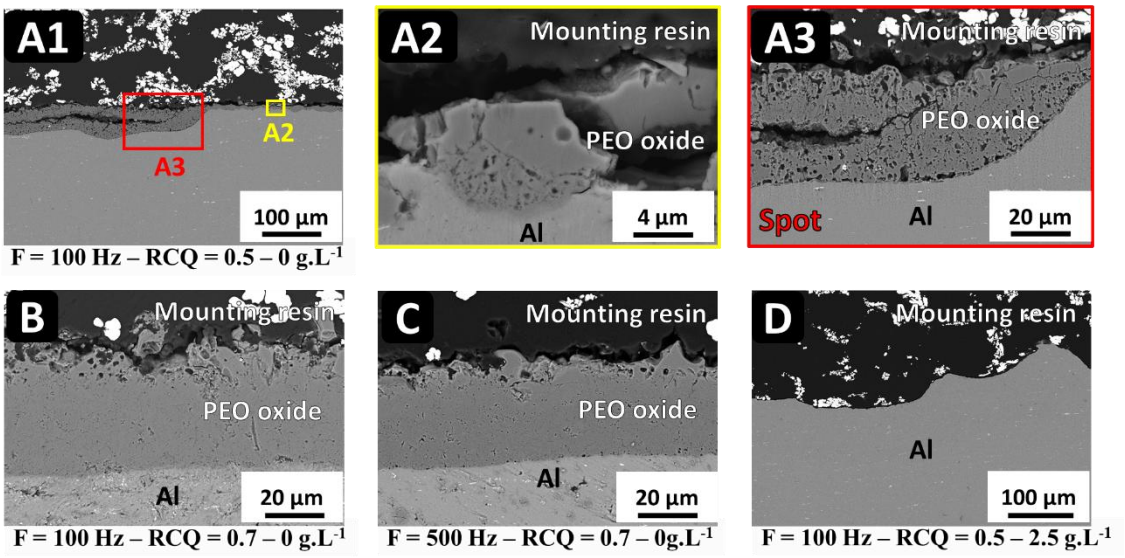
A1
A2
A3
100 µm
F = 100 Hz – RCQ = 0.5 – 0 g.L-1
A2
Mounting resin
PEO oxide
Al
4 µm
A3
Mounting resin
PEO oxide
Spot
Al
20 µm
B
Mounting resin
PEO oxide
Al
20 µm
F = 100 Hz – RCQ = 0.7 – 0 g.L-1
C
Mounting resin
PEO oxide
Al
20 µm
F = 500 Hz – RCQ = 0.7 – 0g.L-1
D
Mounting resin
Al
100 µm
F = 100 Hz – RCQ = 0.5 – 2.5 g.L-1

8

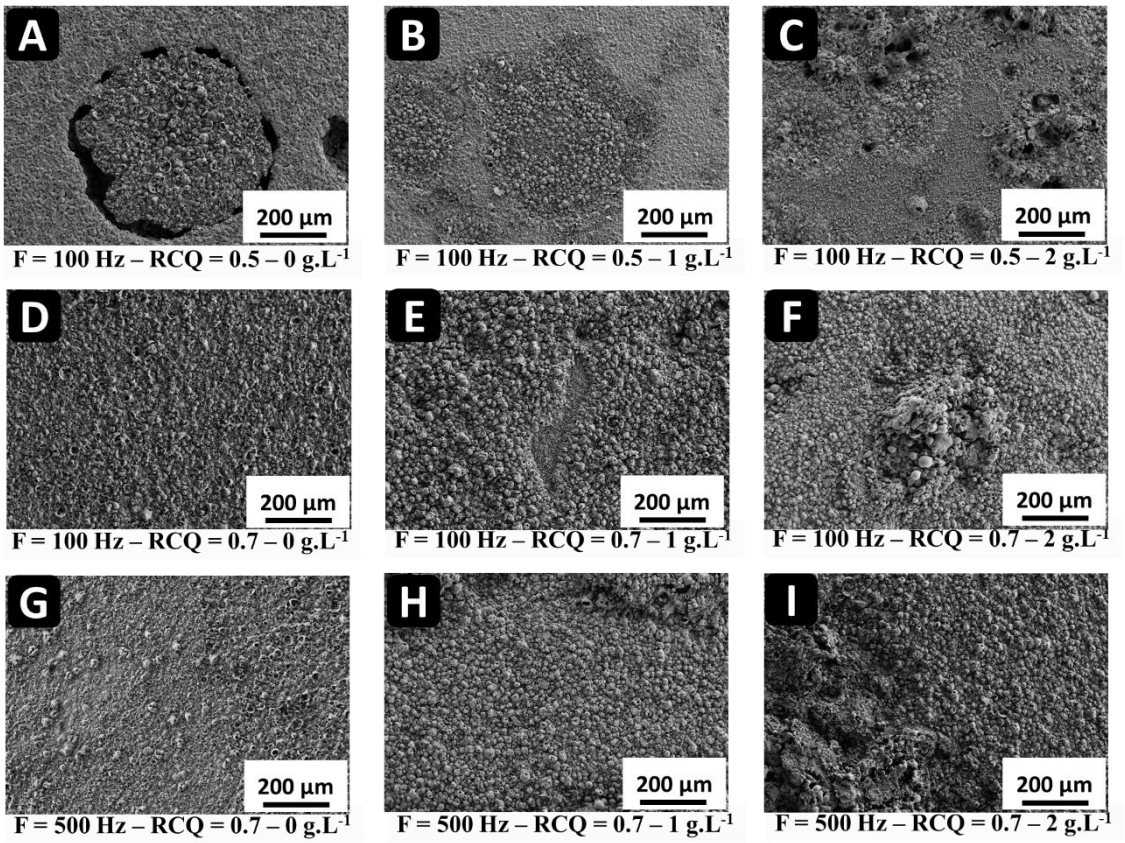
A
200 µm
F = 100 Hz – RCQ = 0.5 – 0 g.L-1
B
200 µm
F = 100 Hz – RCQ = 0.5 – 1 g.L-1
C
200 µm
F = 100 Hz – RCQ = 0.5 – 2 g.L-1
D
200 µm
F = 100 Hz – RCQ = 0.7 – 0 g.L-1
E
200 µm
F = 100 Hz – RCQ = 0.7 – 1 g.L-1
F
200 µm
F = 100 Hz – RCQ = 0.7 – 2 g.L-1
G
200 µm
F = 500 Hz – RCQ = 0.7 – 0 g.L-1
H
200 µm
F = 500 Hz – RCQ = 0.7 – 1 g.L-1
I
200 µm
F = 500 Hz – RCQ = 0.7 – 2 g.L-1

9

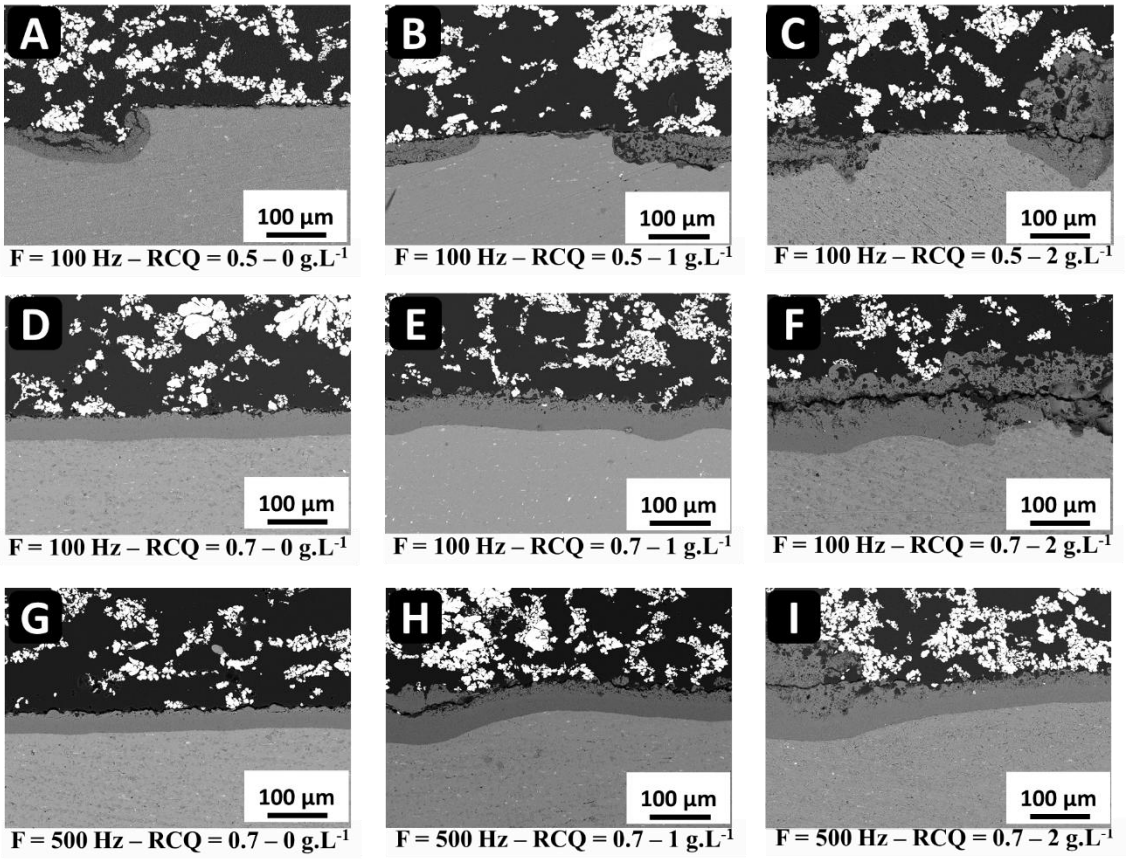
A
100 µm
F = 100 Hz – RCQ = 0.5 – 0 g.L-1
B
100 µm
F = 100 Hz – RCQ = 0.5 – 1 g.L-1
C
100 µm
F = 100 Hz – RCQ = 0.5 – 2 g.L-1
D
100 µm
F = 100 Hz – RCQ = 0.7 – 0 g.L-1
E
100 µm
F = 100 Hz – RCQ = 0.7 – 1 g.L-1
F
100 µm
F = 100 Hz – RCQ = 0.7 – 2 g.L-1
G
100 µm
F = 500 Hz – RCQ = 0.7 – 0 g.L-1
H
100 µm
F = 500 Hz – RCQ = 0.7 – 1 g.L-1
I
100 µm
F = 500 Hz – RCQ = 0.7 – 2 g.L-1

10

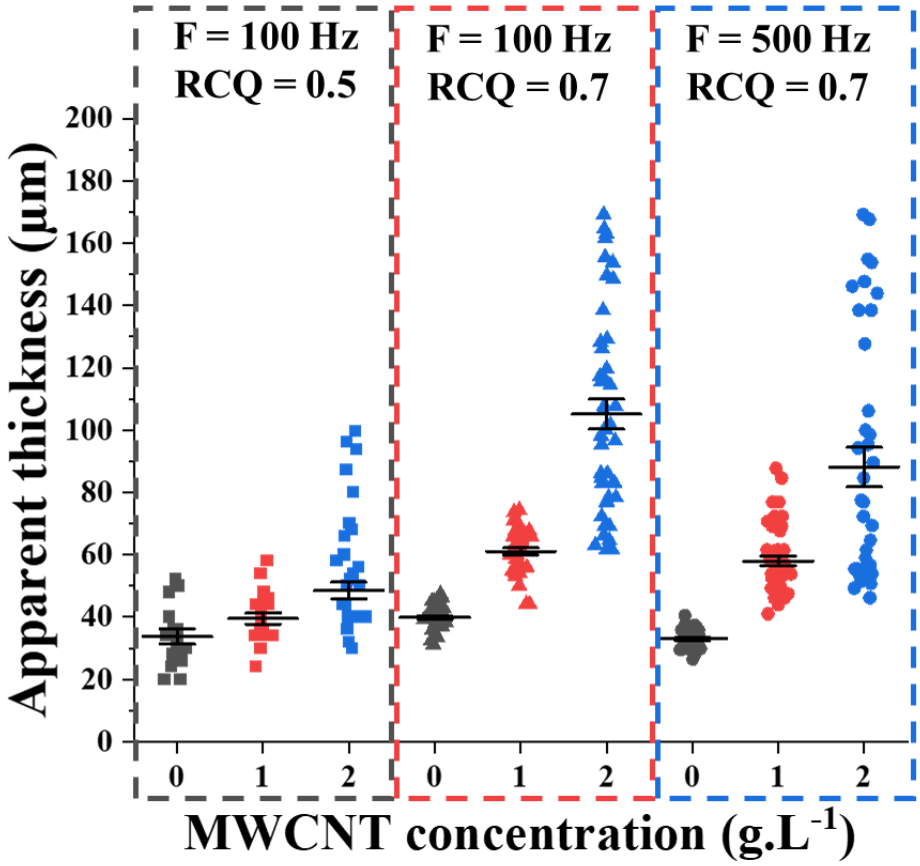
F = 100 Hz
RCQ = 0.5
F = 100 Hz
RCQ = 0.7
F = 500 Hz
RCQ = 0.7
Apparent thickness (µm)
0
20
40
60
80
100
120
140
160
180
200
0
1
2
0
1
2
0
1
2
MWCNT concentration (g.L-1)

11

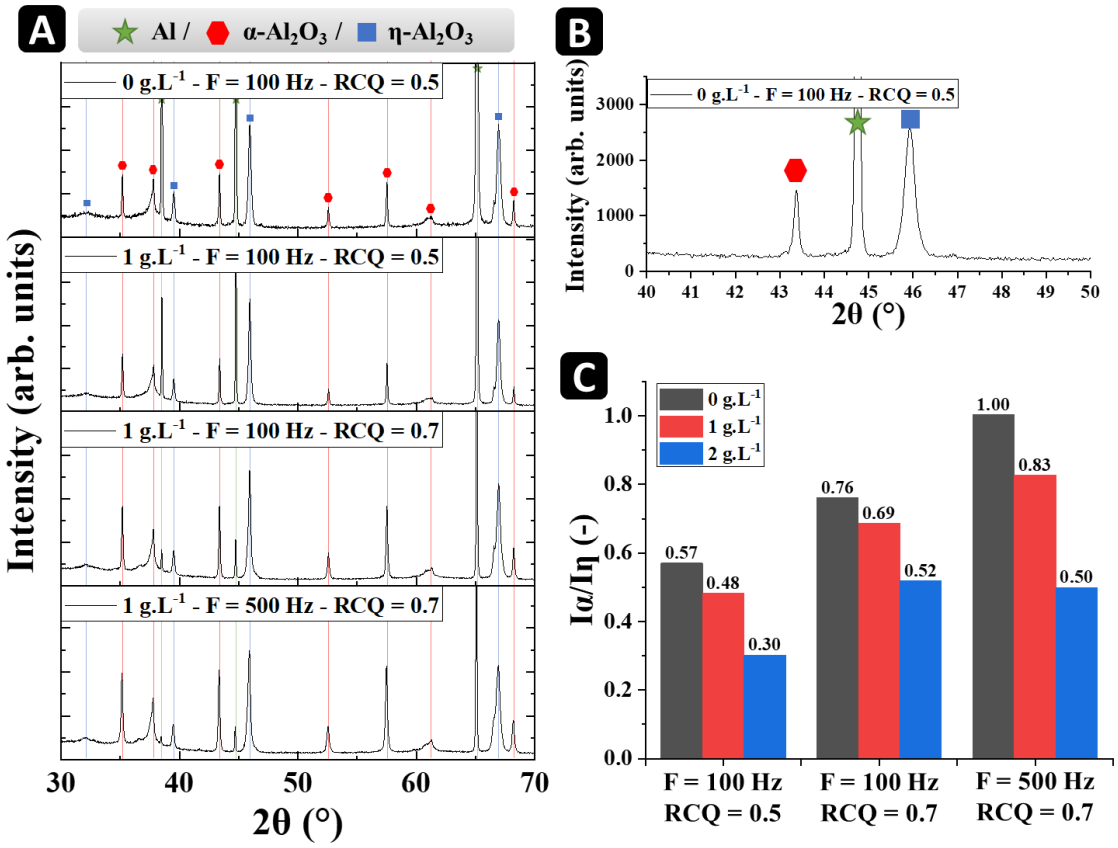
A
Al / α-Al2O3 / η-Al2O3
0 g.L-1 - F = 100 Hz - RCQ = 0.5
1 g.L-1 - F = 100 Hz - RCQ = 0.5
1 g.L-1 - F = 100 Hz - RCQ = 0.7
1 g.L-1 - F = 500 Hz - RCQ = 0.7
Intensity (arb. units)
2θ (°)
B
0 g.L-1 - F = 100 Hz - RCQ = 0.5
Intensity (arb. units)
2θ (°)
C
0 g.L-1
1 g.L-1
2 g.L-1
Iα/Iη (-)
0.57
0.48
0.30
0.76
0.69
0.52
1.00
0.83
0.50
F = 100 Hz
RCQ = 0.5
F = 100 Hz
RCQ = 0.7
F = 500 Hz
RCQ = 0.7

12